

Thermal Behavior and Crystallization of $\text{Fe}_{81-x}\text{Co}_x\text{Zr}_7\text{Nb}_2\text{B}_{10}$ ($x = 2, 4, 6$) Alloys

W.Q. YU, Y.M. SUN, L.H. LIU, L.R. DONG AND Z. HUA*

Key Laboratory of Functional Materials Physics and Chemistry of the Ministry of Education
Jilin Normal University, Siping 136000, Jilin, P.R. China

(Received March 21, 2011; revised version October 19, 2011; in final form November 9, 2011)

Thermal behavior and microstructure of $\text{Fe}_{81-x}\text{Co}_x\text{Zr}_7\text{Nb}_2\text{B}_{10}$ ($x = 2, 4, 6$) alloys were investigated by differential thermal analysis and X-ray diffraction. Both the supercooled liquid region ΔT_x and the first crystallization peak temperature T_{p1} are the lowest and the span ΔT_p between T_{p1} and T_{p2} is the highest when 4 at.% Fe is substituted by Co. The crystallization activation energy E_{p1} for $\text{Fe}_{75}\text{Co}_6\text{Zr}_7\text{Nb}_2\text{B}_{10}$ alloy is the minimum for the heating rates $\nu = 5\text{--}20$ K/min. E_{p1} for $\text{Fe}_{77}\text{Co}_4\text{Zr}_7\text{Nb}_2\text{B}_{10}$ alloy is the minimum for the heating rates $\nu = 20\text{--}50$ K/min. The crystallization processes of $\text{Fe}_{81-x}\text{Co}_x\text{Zr}_7\text{Nb}_2\text{B}_{10}$ ($x = 2, 4, 6$) amorphous alloys are similar on the whole, which is as follows: amorphous \rightarrow amorphous + $\alpha\text{-Fe}(\text{Co}) \rightarrow \alpha\text{-Fe}(\text{Co}) + \text{Fe}_3\text{Zr} + \text{Fe}_2\text{Nb}_{0.4}\text{Zr}_{0.6}$.

PACS: 65.60.+a, 61.43.Dg

1. Introduction

Nanocrystalline soft magnetic alloys have attracted a great deal of attention from scientists over the past several decades. Among the soft magnetic nanocrystalline systems, considerable attention is devoted to the Fe-based alloys [1–10]. The microstructure, magnetic property and crystallization behavior of Fe-based alloys have been investigated in detail. The study of the crystallization behavior is very important in understanding the thermal stability of the amorphous phase [6]. The glass forming ability (GFA) of alloys can be evaluated by a temperature span of the supercooled liquid region ΔT_x (difference between the glass transition temperature T_g and the onset crystallization temperature T_x). The wider is the ΔT_x , the greater is the GFA [11]. The purpose of this study is to investigate the thermal behavior and crystallization of $\text{Fe}_{81-x}\text{Co}_x\text{Zr}_7\text{Nb}_2\text{B}_{10}$ ($x = 2, 4, 6$) amorphous alloys.

2. Experimental details

$\text{Fe}_{81-x}\text{Co}_x\text{Zr}_7\text{Nb}_2\text{B}_{10}$ ($x = 2, 4, 6$) amorphous alloys were prepared by melt-spinning and annealed at 803, 873, 943 and 1023 K for 40 min. The microstructure was examined by X-ray diffraction (XRD, D/max 2500/PC, Cu K_α , $\lambda = 1.5406$ Å). Thermal analysis was carried out in the Perkin Elmer TG/DTA-6300 instrument at different heating rates (5, 10, 20, 30 and 50 K/min). Detailed thermal analysis of samples reveals a spectrum of values for glass transition temperature T_g , onset crystallization temperature T_x , the first crystallization peak temperature T_{p1} and the second crystallization peak temperature

T_{p2} . The GFA of alloys can be evaluated by a temperature span of the supercooled liquid region ΔT_x .

3. Results and discussion

Figure 1a–c shows the differential thermal analysis (DTA) traces of $\text{Fe}_{81-x}\text{Co}_x\text{Zr}_7\text{Nb}_2\text{B}_{10}$ ($x = 2, 4, 6$) amorphous alloys at different heating rates. The ther-

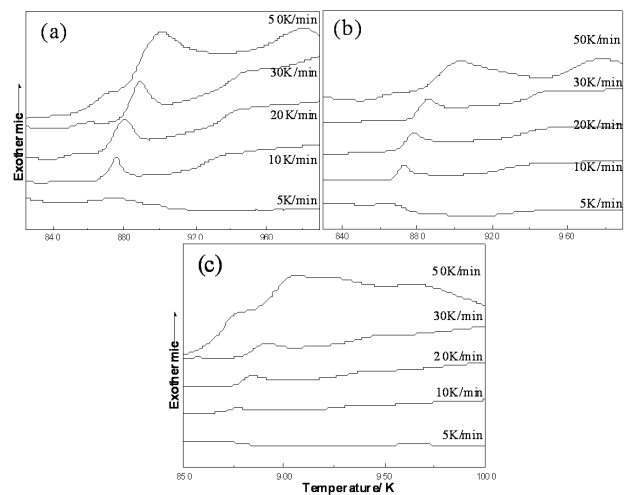


Fig. 1. DTA traces of $\text{Fe}_{81-x}\text{Co}_x\text{Zr}_7\text{Nb}_2\text{B}_{10}$ [$x = 2$ (a), 4 (b), 6 (c)] amorphous alloys at different heating rates.

modynamic parameters all increase with increasing heating rate. The first crystallization peaks T_{p1} and the second crystallization peak T_{p2} obtained at different heating rates are listed in Table I. Figure 2 shows the DTA traces of $\text{Fe}_{81-x}\text{Co}_x\text{Zr}_7\text{Nb}_2\text{B}_{10}$ ($x = 2, 4, 6$) amorphous alloys at a heating rate of 30 K/min. It can be seen that a low exothermic peak precedes the main crystallization

* corresponding author; e-mail: huazhong196110@163.com

peak, which is supposed to be a pre-crystallization effect [12]. T_g , T_x , ΔT_x , T_{p1} and ΔT_p (difference between T_{p1} and T_{p2}) of three amorphous alloys at a heating rate of 30 K/min as a function of Co content are shown in Fig. 3. Both ΔT_x and T_{p1} are the lowest and the span

ΔT_p is the highest when the partial substitution of Fe by Co is of the amount of 4 at.%. The heating rate has an important influence on the crystallization activation energy [13].

TABLE I

The first crystallization peak T_{p1} and the second crystallization peak T_{p2} of $\text{Fe}_{81-x}\text{Co}_x\text{Zr}_7\text{Nb}_2\text{B}_{10}$ [$x = 2$ (a), 4 (b), 6 (c)] amorphous alloys obtained at different heating rates.

V [K/min]	T_{p1} [K]					T_{p2} [K]				
	5	10	20	30	50	5	10	20	30	50
a	872.0	877.9	882.8	890.6	900.9	—	935.9	945.2	949.7	980.7
b	866.9	873.0	878.1	885.3	898.6	—	939.2	950.5	952.4	978.5
c	868.1	877.0	884.2	891.6	900.5	—	932.7	943.0	948.6	968.8

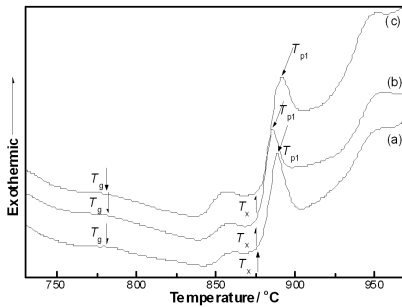


Fig. 2. DTA traces of $\text{Fe}_{81-x}\text{Co}_x\text{Zr}_7\text{Nb}_2\text{B}_{10}$ [$x = 2$ (a), 4 (b), 6 (c)] amorphous alloys at a heating rate of 30 K/min.

The Kissinger plots for T_{p1} are shown in Fig. 4. The crystallization activation energies E for the crystallization peaks T_p are calculated using the Kissinger equation [14] by plotting $\ln(\nu/T^2)$ versus $1/T$ (a straight line with the slope of E/R can be obtained), where R is the gas constant, ν is the heating rate (K/min) and T is a specific absolute temperature such as crystallization peak T_p . A critical heating rate, $\nu_{\text{crit}} = 20$ K/min, is evident. The Kissinger plot is divided into two intervals according to the different slope. Yuan et al. [13] studied the non-isothermal crystallization of $\text{Co}_{43}\text{Fe}_{20}\text{Ta}_{5.5}\text{B}_{31.5}$ amorphous alloy and reported similar phenomenon. At low heating rates, the crystallization activation energy is composed of the activation energy of nucleation and the activation energy of growth. At high heating rates, the crystallization activation energy is mainly composed of the activation energy of growth. The crystallization activation energies E_{p1} are listed in Table II. E_{p1} for $\text{Fe}_{75}\text{Co}_6\text{Zr}_7\text{Nb}_2\text{B}_{10}$ alloy is the minimum for the heating rates $\nu = 5\text{--}20$ K/min. E_{p1} for $\text{Fe}_{77}\text{Co}_4\text{Zr}_7\text{Nb}_2\text{B}_{10}$ alloy is the minimum for the heating rates $\nu = 20\text{--}50$ K/min.

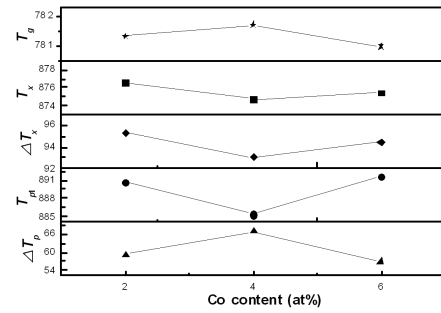


Fig. 3. T_g , T_x , ΔT_x , T_{p1} and ΔT_p of $\text{Fe}_{81-x}\text{Co}_x\text{Zr}_7\text{Nb}_2\text{B}_{10}$ ($x = 2, 4, 6$) amorphous alloys at a heating rate of 30 K/min as a function of Co content.

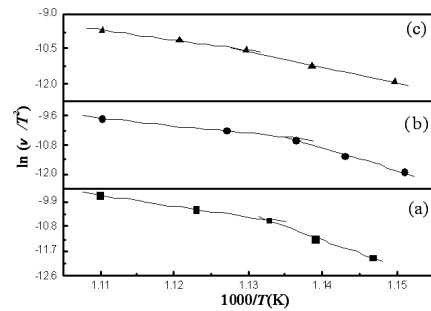


Fig. 4. The Kissinger plots for $\text{Fe}_{81-x}\text{Co}_x\text{Zr}_7\text{Nb}_2\text{B}_{10}$ [$x = 2$ (a), 4 (b), 6 (c)] amorphous alloys.

XRD patterns of $\text{Fe}_{81-x}\text{Co}_x\text{Zr}_7\text{Nb}_2\text{B}_{10}$ ($x = 2, 4, 6$) alloys corresponding to different annealing temperatures are shown in Fig. 5a–c. The crystallization processes of the three alloys are similar on the whole. No crystalline peaks are observed for three alloys as-quenched, which in-

TABLE II

The crystallization activation energies E_{p1} of $\text{Fe}_{81-x}\text{Co}_x\text{Zr}_7\text{Nb}_2\text{B}_{10}$ ($x = 2, 4, 6$) amorphous alloys.

	E_{p1} [KJ/mol]	
	$\nu = 5\text{--}20$ K/min	$\nu = 20\text{--}50$ K/min
$\text{Fe}_{79}\text{Co}_2\text{Zr}_7\text{Nb}_2\text{B}_{10}$	803.3 ± 46.5	319.5 ± 2.6
$\text{Fe}_{77}\text{Co}_4\text{Zr}_7\text{Nb}_2\text{B}_{10}$	766.1 ± 43.0	273.6 ± 28.2
$\text{Fe}_{75}\text{Co}_6\text{Zr}_7\text{Nb}_2\text{B}_{10}$	531.8 ± 36.1	355.6 ± 30.9

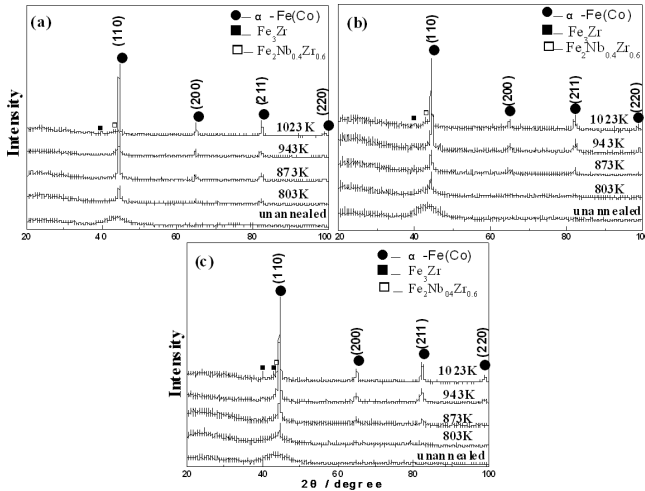


Fig. 5. XRD patterns of $\text{Fe}_{81-x}\text{Co}_x\text{Zr}_7\text{Nb}_2\text{B}_{10}$ [$x = 2$ (a), 4 (b), 6 (c)] alloys corresponding to different annealing temperatures.

indicate that the three alloys as-quenched all exhibit amorphous character. Annealing at 873 K induces the precipitation of $\alpha\text{-Fe(Co)}$ phase from the amorphous matrix. The intensity of $\alpha\text{-Fe(Co)}$ diffraction peaks increases with increasing annealing temperature. The $\alpha\text{-Fe(Co)}$, Fe_3Zr and $\text{Fe}_2\text{Nb}_{0.4}\text{Zr}_{0.6}$ phases are observed at the final crystallization stage. There are two exothermal peaks after pre-crystallization effect in the DTA curves. The first exothermal peak in the DTA curve corresponds to the precipitation of $\alpha\text{-Fe(Co)}$ phase. The second exothermal peak corresponds to the precipitations of Fe_3Zr and $\text{Fe}_2\text{Nb}_{0.4}\text{Zr}_{0.6}$ phases. The crystallization processes of the three alloys are as follows: amorphous \rightarrow amorphous + $\alpha\text{-Fe(Co)}$ \rightarrow $\alpha\text{-Fe(Co)}$ + Fe_3Zr + $\text{Fe}_2\text{Nb}_{0.4}\text{Zr}_{0.6}$.

4. Conclusions

Thermal behavior and crystallization of $\text{Fe}_{81-x}\text{Co}_x\text{Zr}_7\text{Nb}_2\text{B}_{10}$ ($x = 2, 4, 6$) alloys were investigated in this work. Both the supercooled liquid region ΔT_x and the first crystallization peak temperature T_{p1} are the lowest and the span ΔT_p between T_{p1} and T_{p2} is the highest when 4 at.% Fe is substituted

by Co. E_{p1} for $\text{Fe}_{75}\text{Co}_6\text{Zr}_7\text{Nb}_2\text{B}_{10}$ alloy is the minimum for the heating rates $\nu = 5\text{--}20$ K/min. E_{p1} for $\text{Fe}_{77}\text{Co}_4\text{Zr}_7\text{Nb}_2\text{B}_{10}$ alloy is the minimum for the heating rates $\nu = 20\text{--}50$ K/min. There are two exothermal peaks after pre-crystallization effect in the DTA curves. The first exothermal peak in the DTA curve corresponds to the precipitation of $\alpha\text{-Fe(Co)}$. The second exothermal peak corresponds to the precipitations of Fe_3Zr and $\text{Fe}_2\text{Nb}_{0.4}\text{Zr}_{0.6}$ phases. The crystallization processes of $\text{Fe}_{81-x}\text{Co}_x\text{Zr}_7\text{Nb}_2\text{B}_{10}$ ($x = 2, 4, 6$) amorphous alloys are similar on the whole, which is as follows: amorphous \rightarrow amorphous + $\alpha\text{-Fe(Co)}$ \rightarrow $\alpha\text{-Fe(Co)}$ + Fe_3Zr + $\text{Fe}_2\text{Nb}_{0.4}\text{Zr}_{0.6}$.

Acknowledgments

This work was funded by Science and Technology Development Project of Jilin Province (No. 201105083), Science and Technology Studying Project of “12th five-year” Office of Education of Jilin Province (No. 2011-158) and Graduate Innovative Research Programs of Jilin Normal University (No. 201103).

References

- [1] B. Movahedi, M.H. Enayati, C.C. Wong, *Mater. Lett.* **64**, 1055 (2010).
- [2] J.S. Blázquez, J.J. Ipus, M. Millán, V. Franco, A. Conde, D. Oleszak, T. Kulik, *J. Alloys Comp.* **469**, 169 (2009).
- [3] M. Pilar, L. Escoda, J.J. Suñol, J.M. Greneche, *J. Magn. Magn. Mater.* **320**, e823 (2008).
- [4] K. Zhang, Z. Lv, B. Yao, D. Wang, *J. Non-Cryst. Solids* **352**, 78 (2006).
- [5] M.N. Gona, S. Yanase, S. Hashi, Y. Okazaki, *J. Magn. Magn. Mater.* **254**, 466 (2003).
- [6] Y.J. Liu, I.T.H. Chang, *Mater. Sci. Eng. A* **325**, 25 (2002).
- [7] A. Makino, T. Bitoh, A. Kojima, A. Inoue, T. Masumoto, *Mater. Sci. Eng. A* **304-306**, 1083 (2001).
- [8] A. Makino, T. Bitoh, A. Kojima, A. Inoue, T. Masumoto, *J. Appl. Phys.* **87**, 7100 (2000).
- [9] D. Arvindha Babu, B. Majumdar, R. Sarkar, M. Manivel Raja, D. Akhtar, *J. Mater. Res.* **26**, 2065 (2011).
- [10] K. Suzuki, N. Kataoka, A. Inoue, A. Makino, T. Masumoto, *Mater. Trans. Jpn. Inst. Met.* **31**, 743 (1990).
- [11] A. Inoue, *Acta Mater.* **48**, 279 (2000).
- [12] E. Illeková, P. Švec, M. Miglierini, *J. Non-Cryst. Solids* **353**, 3342 (2007).
- [13] Z.Z. Yuan, X.D. Chen, B.X. Wang, Y.J. Wang, *J. Alloys Comp.* **407**, 163 (2006).
- [14] H.E. Kissinger, *Anal. Chem.* **29**, 1702 (1957).